frontiers | Frontiers in Electronic Materials

TYPE Original Research
PUBLISHED 13 December 2022
DOI 10.3389/femat.2022.1044620

OPEN ACCESS

EDITED BY
Audrey Grockowiak,
National Center for Research in Energy and Materials, Brazil

REVIEWED BY
Minghu Fang,
Zhejiang University, China
Yanpeng Qi,
ShanghaiTech University, China

*CORRESPONDENCE
K. Shrestha,
kshrestha@wtamu.edu

SPECIALTY SECTION
This article was submitted to Superconducting Materials, a section of the journal Frontiers in Electronic Materials

RECEIVED 14 September 2022
ACCEPTED 23 November 2022
PUBLISHED 13 December 2022

CITATION
Shrestha K, Deng LZ, Lv B and Chu CW (2022), Evolution of magnetic properties in iron-based superconductor Eu-doped $CaFe_2As_2$.
Front. Electron. Mater. 2:1044620.
doi: 10.3389/femat.2022.1044620

Evolution of magnetic properties in iron-based superconductor Eu-doped $CaFe_2As_2$

K. Shrestha[1]*, L. Z. Deng[2], B. Lv[3] and C. W. Chu[2,4]

[1]Department of Chemistry and Physics, West Texas A&M University, Canyon, TX, United States, [2]Texas Center for Superconductivity and Department of Physics, University of Houston, Houston, TX, United States, [3]Department of Physics, The University of Texas at Dallas, Richardson, TX, United States, [4]Lawrence Berkeley National Laboratory, Berkeley, CA, United States

This work presents the evolution of magnetic properties of $Eu_xCa_{1-x}Fe_2As_2$ ($0 \leq x \leq 1$, ECFA) samples. Unlike the resistivity data, that for magnetic susceptibility χ (T) does not show any clear evidence of the spin density wave (SDW) transition. When the Curie-Weiss contribution is subtracted, a weak anomaly appears at a temperature close to the SDW transition temperature (T_{SDW}) determined from the resistivity data. To understand the magnetic orders arising from Fe-moments and Eu^{2+} spins order, we have studied the doping dependence of T_{SDW} and Eu^{2+} antiferromagnetic order T_N. It is found that T_{SDW} increases almost linearly with increasing x and remains nearly unchanged above $x \sim 0.4$, whereas T_N first appears at $x \sim 0.4$ and varies almost linearly with further increasing x. These observations suggest that magnetic orders due to two sublattices are coupled to each other. The results discussed here are helpful for understanding the magnetic properties of ECFA and other iron-based superconductors.

KEYWORDS

iron-based superconductors, spin-density wave order, antiferromagnetic order, Curie-Weiss law, magnetic susceptability

Introduction

Iron-based superconductors (IBSs) have continuously served as a platform for exploring novel experimental tools and theoretical approaches since their discovery, especially in studies on the impact of magnetic fluctuations and quantum criticality (Chen et al., 2008a; Hsu et al., 2008; Kamihara et al., 2008; Wang et al., 2012; Deng et al., 2014; Lei et al., 2016; Komedera et al., 2018; Deng et al., 2021; Fernandes et al., 2022). The Fe-magnetic moments appear as a spin density wave (SDW) and, in general, superconductivity emerges when the SDW order is suppressed either by appropriate chemical doping or by applying external pressure (Chen et al., 2008b; Rotter et al., 2008; Takahashi et al., 2008). Thin-film FeSe/STO grown by molecular beam epitaxy (MBE) has exhibited interface-enhanced superconductivity with a T_c above 40 K (Wang et al., 2012; Deng et al., 2014). More recently, a T_c of 38 K was retained in FeSe single crystals at ambient pressure via pressure-quenching (Deng et al., 2021). Defects have also been reported to play an important role in the superconductivity of IBSs (Deng et al., 2016).

$CaFe_2As_2$ (Ca122) and $EuFe_2As_2$ (Eu122) are two members of the "122" IBS family [$(AE)Fe_2As_2$ (AE = Ca, Ba, Sr, and Eu)] and show SDW transitions at T_{SDW} ~ 165 K and 190 K, respectively (Park et al., 2008; Torikachvili et al., 2008; Lee et al., 2009). At the SDW transition, which appears as a sharp upturn in the resistivity data (Park et al., 2008; Lee et al., 2009; Lv et al., 2011; Shrestha et al., 2020), the material undergoes structural (from the tetragonal to the orthorhombic phase) and magnetic phase (antiferromagnetic ordering of Fe-moments) transitions simultaneously. In Ca122, there exists an additional structural transition near 100 K to the "collapsed-tetragonal" (cT) phase under a moderate pressure of ~ 0.4 GPa before the superconductivity transition occurs. However, under truly hydrostatic pressure, no superconductivity is observed in Ca122 (Yu et al., 2009). A higher T_c up to 49 K was achieved in this system by chemical doping (Lv et al., 2011) with rare-earth elements. Our group recently reported (Zhao et al., 2016) that the T_c of Ca122 can be raised as high as 25 K using a proper annealing procedure. Another 122 IBS, Eu122, in addition to having a high-temperature SDW transition, exhibits an anomaly near T_N ~ 20 K due to its Eu^{2+} antiferromagnetic (AFM) order (Ren et al., 2008). It does not show any signature of superconductivity at ambient condition, but it can be turned into a superconductor either by chemical doping [with K (Jeevan et al., 2008) (T_c ~ 32 K), with Na (Qi et al., 2008) (T_c ~ 35 K), through Co or La substitutions (He et al., 2010; Ying et al., 2010; Zhang et al., 2012), etc.] or by the application of external high pressure (Terashima et al., 2009; Kurita et al., 2011).

Here, we explore the evolution of the electrical transport and magnetic properties of Eu-doped Ca122 [$Eu_xCa_{1-x}Fe_2As_2$ ($0 \leq x \leq 1$, ECFA)]. We recently reported (Shrestha et al., 2020) detailed electrical transport properties of ECFA at ambient and under high-pressure. Here we focus on how its magnetic properties evolve with varied Eu-doping. We observe that, unlike in the measurement of resistivity, the magnetic susceptibility data does not show a visible anomaly resulting from the SDW transition. We find that a tiny anomaly near the SDW transition appears only after subtracting the Curie-Weiss (CW) contribution of the Eu^{+2} moments.

Experimental details

Large, high-quality single crystals of ECFA were grown using the FeAs flux technique. Starting materials were placed in an

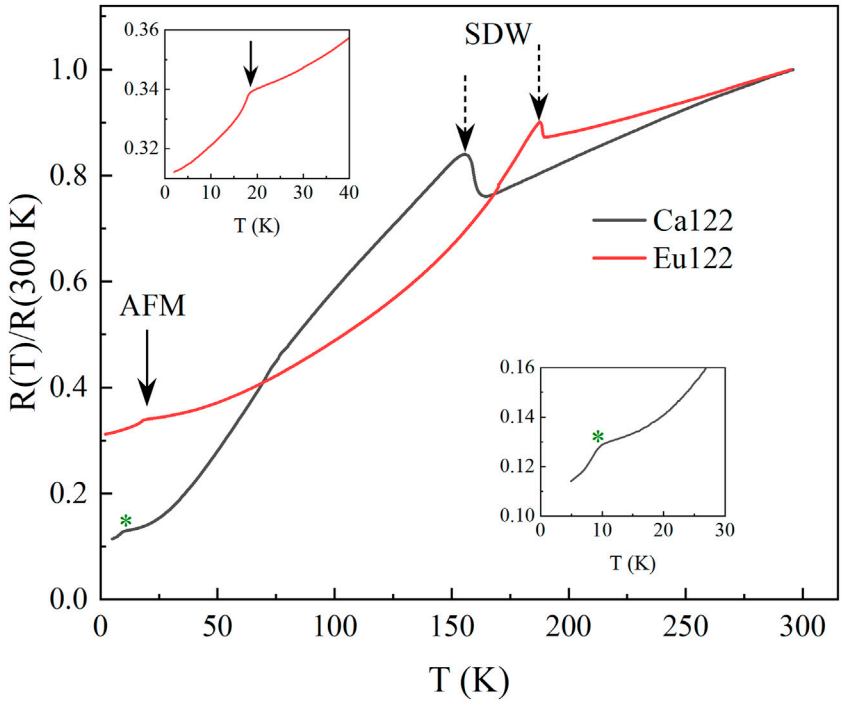

FIGURE 1
Electrical Resistance. Normalized electrical resistance vs. temperature for Ca122 and Eu122. Both samples show a clear anomaly, near 160 K and 190 K for Ca122 and Eu122, respectively, and indicated by dashed arrows, that arises due the SDW transition. The tiny kink near 19 K for Eu122, as indicated by the solid arrow, is due to the Eu^{2+} AFM order. A small drop in resistance for Ca122 near 10 K, as denoted by an asterisk, is likely due to the superconducting transition (see the text). Upper inset: magnified view of the Eu^{2+} AFM transition in Eu122. Lower inset: magnified view of the low-temperature drop in resistance for Ca122.

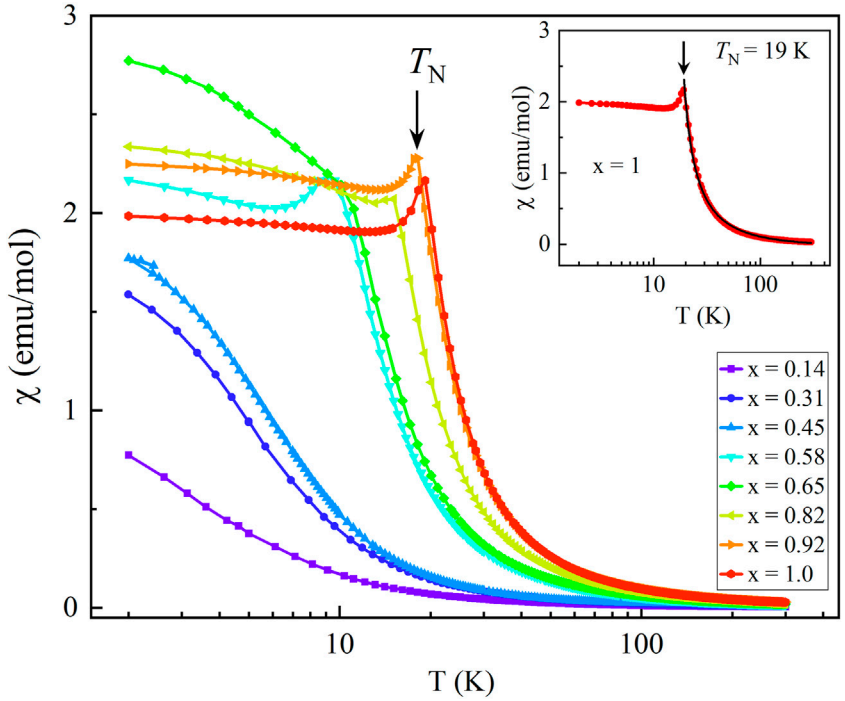

FIGURE 2
Magnetic susceptibility. Magnetic susceptibility (χ) vs. T for ECFA samples with different amounts of Eu doping ($0.14 \leq x \leq 1$. χ (T) increases gradually with decreasing temperature. The low-temperature anomalies, $T_N \sim 10$–19 K, arise due to the Eu^{2+} AFM order, as indicated by the arrow. Inset: χ (T) data for $EuFe_2As_2$ ($x = 1$). The solid black curve is the best-fit curve using the Curie-Weiss model Eq. 1. The x-axis is in the logarithmic scale for better visibility of T_N.

alumina crucible that was sealed inside a small silica tube under a reduced Ar atmosphere. The small silica tube was subsequently sealed inside a larger silica tube under vacuum. The assembly was first heated at a temperature of 1,100°C and then slowly cooled down at a rate of 2°C/h. The sample preparation and preliminary characterization details are provided in our previous report (Shrestha et al., 2020). Electrical transport measurement were carried out in a physical property measurement system (PPMS, Quantum Design). A shiny crystal was selected and four platinum wires were attached to its flat surface using silver paint. Magnetic measurements from room temperature down to 2 K were carried out using a magnetic property measurement system (MPMS, Quantum Design). A plate-like sample was placed inside a gelatin capsule that was subsequently attached to a plastic straw. A small magnetic field value of 0.1 T was applied along the c-axis to induce a magnetic moment in the sample.

Results and discussion

Figure 1 shows the temperature-dependent electrical resistance of Ca122 and Eu122. The resistance is normalized to the room-temperature value. Each sample shows a clear upturn anomaly near $T_{SDW} \sim 160$ K (Ca122) or 190 K (Eu122) that arises due to the SDW transition, as indicated by the dashed arrows. These T_{SDW} values are consistent with previously reported data (Park et al., 2008; Torikachvili et al., 2008; Lee et al., 2009; Lv et al., 2011). Moreover, there is a tiny kink near $T_N \sim 19$ K in the Eu122 results (indicated by the solid arrow), which can be more clearly observed in the magnified view shown in the upper inset to Figure 1. This anomaly arises due to the AFM ordering of Eu^{2+} spin moments (Shrestha et al., 2020). For Ca122, there is a small drop in the resistance value near 10 K, indicated by an asterisk and more clearly visible in the magnified view shown in the lower inset to Figure 1. Under application of external pressure, Ca122 enters into the superconducting state with a transition temperature $T_c \sim 10$ K (Park et al., 2008; Torikachvili et al., 2008; Lee et al., 2009). Therefore, this tiny drop in resistance could be due to the onset of the superconducting transition.

Figure 2 shows the temperature-dependent magnetic susceptibility (χ) of ECFA samples with different amounts of Eu doping (x). χ (T) increases gradually with decreasing temperature and exhibits a distinct anomaly near $T_N \sim$

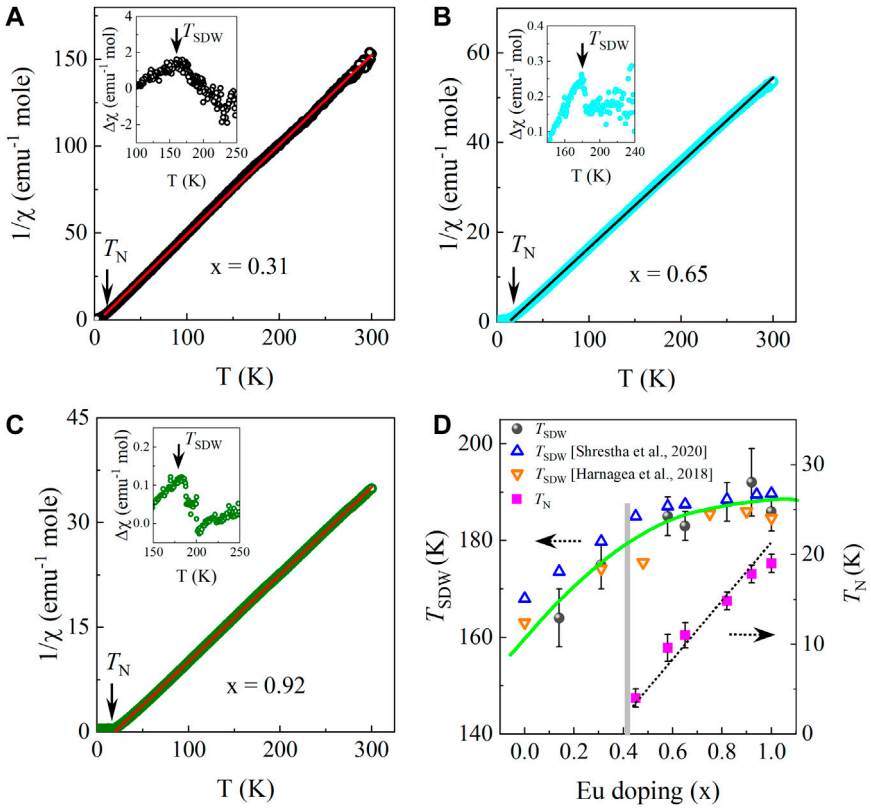

FIGURE 3
Curie-Weiss fit. Inverse susceptibility, $1/\chi$, vs. T for ECFA samples at **(A)** $x = 0.31$, **(B)** $x = 0.65$, and **(C)** $x = 0.92$.$1/\chi$ increases linearly with T, consistent with Curie-Weiss behavior. The arrows show the AFM due to the Eu^{2+} spins. The solid lines are the best-fit lines using the Curie-Weiss law Eq. 1. The insets in **(A)–(C)** display the respective $\Delta\chi$ vs. T plots showing the T_{SDW} transitions, as indicated by the arrow in each. **(D)** T_{SDW} (solid spheres) and T_N (solid squares) vs. x for ECFA samples. Open upright and inverted triangles are T_{SDW} data from Refs (Shrestha et al., 2020). and (Harnagea et al., 2018), respectively. T_{SDW} increases rapidly with increasing x and then slowly saturates to $T_{SDW} \sim 190$ K above $x \sim 0.4$. The error bars are taken as the half-width of the transition. The vertical solid stripe and solid curve are guides to the eye. T_N first appears at $x \sim 0.4$ and increases almost linearly with further increasing x, as indicated by the dotted line.

10–19 K, as indicated by the arrow. This transition arises due to the Eu^{2+} AFM order (Ren et al., 2008; Zhang et al., 2012; Maiwald and Gegenwart, 2017). T_N is prominent at higher x, and it shifts toward lower temperatures at lower x. For $x = 1$, $T_N \sim 19$ K, which is consistent with previously reported T_N values (Ren et al., 2008; Zhang et al., 2012; Maiwald and Gegenwart, 2017). Our recent rigorous electrical transport and magnetic studies (Shrestha et al., 2020) showed that T_N varies linearly with x. Here, the temperature dependence of χ (T) can be described by the Curie-Weiss (CW) law Eq. 1 as shown in the inset to Figure 2 for the $x = 1$ sample. The CW law (Ashcroft and Mermin, 1976; Kittel, 2006) is expressed as

$$\chi = \frac{C}{T - \theta}, \tag{1}$$

where C and θ are the Curie-Weiss constant and the Weiss temperature, respectively. Here, C is directly proportional to the effective magnetic moment (μ_{eff}) of the sample. Therefore, by fitting the temperature-dependent χ (T) data, we can estimate μ_{eff} and θ of the ECFA samples.

Figures 3A–C shows the $1/\chi$ (T) plots for selected ECFA samples. $1/\chi$ (T) varies linearly at high temperatures, but anomalies corresponding to the Eu^{2+} AFM order occur at low temperatures, as indicated by arrows. The solid lines represent the best-fit to the CW law using Eq. 1. As seen in Figures 3A–C, the temperature-dependent susceptibility data can be well explained by the CW law. It is important to note that there is no clear evidence of the SDW transition in any of the ECFA samples studied [neither in Figure 2 nor in Figures 3A–C] due to Fe-moments in our susceptibility data. In previous studies (Ren et al., 2008; Jiang et al., 2009), the same issue of being unable to observe a clear SDW transition in the magnetization data was reported, but it could be observed after subtracting the CW contribution of the Eu^{2+} moments. Therefore, we have followed the same approach and calculated $\Delta\chi$ (T) by subtracting the CW contribution of the

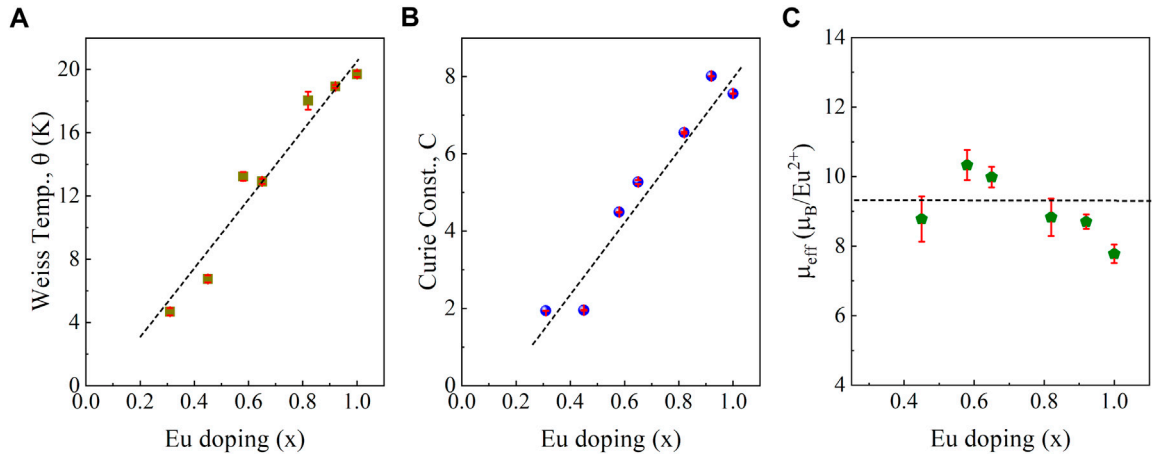

FIGURE 4
Weiss temperature, Curie-constant, and effective moment. The best-fit parameters **(A)** θ (K) and **(B)** C plotted as functions of Eu doping (x). Both θ and C vary nearly linearly with Eu doping, as shown by the dashed lines. **(C)** μ_{eff} per Eu^{2+} ion at various Eu content. Although C increases linearly with increasing x, μ_{eff} per Eu^{2+} ion does not show a clear dependence on x, and its value varies between ~ 8–10 μ_B).

Eu^{2+} moments. As shown in the insets to Figures 3A–C, there is a tiny but distinguishable anomaly at T_{SDW} ~ 165–185 K. These T_{SDW} values are in close agreement with those previously reported based on resistivity and magnetization measurements (Jiang et al., 2009; Harnagea et al., 2018; Tran et al., 2018; Shrestha et al., 2020). We subsequently determined T_{SDW} for various ECFA samples and plotted it as a function of Eu doping. As shown in Figure 3D, T_{SDW} (x) initially increases rapidly with increasing x, gradually increases with further increasing in x above x ~ 0.4, and then saturates to the value of 190 K. As mentioned in the Introduction, ECFA serves as a special platform that has two magnetic orders, one from Fe-moments (SDW order) and another due to Eu^{2+} spins (AFM order). To confirm the interaction between these orders, we have also plotted T_N vs. x on the right y-axis of Figure 3D. As seen in Figure 3D, with decreasing x, T_{SDW} remains almost unchanged until the Eu^{2+} moment order is destroyed at x ~ 0.4. This suggests that the magnetic orders of the two sublattices are coupled to one another.

From the CW-fitting above, we have obtained the best-fit parameters C = (7.94 ± 0.001) emu K/mole and θ = (19.36 ± 0.13) K for x = 0.92. From the C value obtained, we have estimated the effective magnetic moment of Eu^{2+}, μ_{eff} = (7.97 ± 0.10) μ_B. These values are comparable with those previously reported (Jiang et al., 2009; Harnagea et al., 2018; Tran et al., 2018) for a similar Eu-doping level. The positive θ value implies ferromagnetic (FM) interaction between Eu^{2+} moments. Resonant X-ray scattering (Herrero-Martín et al., 2009) and neutron diffraction data (Xiao et al., 2009; Xiao et al., 2010) have also shown that Eu^{2+} spins on the same plane have FM interaction, whereas they have weak AFM coupling across the plane. The Eu-doping-dependent best-fit parameters were calculated for various ECFA samples and are presented in Figure 4.

Figure 4A shows the variation of the best-fit of parameter θ with x. For x = 0.31, θ = (4.68 ± 0.23) K, and it increases almost linearly with further increasing Eu doping. At x = 1, θ = (19.71 ± 0.19). This θ value is comparable with those of 20.3 K reported by Harnagea et al. (2018) and 19.7 K reported by Jiang et al. (2009). Similarly, the Eu-doping-dependent best fit of C is shown in Figure 4B and has nearly linear dependence on x. Figure 4C displays μ_{eff} per Eu^{2+} ion at various Eu content and shows that, although C increases linearly with x, μ_{eff} per Eu^{2+} ion does not exhibit any clear Eu-doping dependence. Its value changes between ~ 8–10 μ_B.

The doping effect on 122 IBSs has been studied extensively using both rare-earth metals (RE = La, Pr, Nd, etc.) (Qi et al., 2008; Gao et al., 2011; Lv et al., 2011; Saha et al., 2012; Ying et al., 2012) and alkali metals (A = K and Na) (Rotter et al., 2008; Sasmal et al., 2008; Zhao et al., 2010). Replacing a divalent AE^{2+} ion with a trivalent RE^{3+} (or a univalent A^{+}) in a 122 IBS serves as electron doping (or hole doping) and tunes the electronic properties of the system. In both cases (electron and hole doping), the SDW order is gradually suppressed, and the superconducting phase has been stabilized in the 122 system with a maximum T_c of 49 K (for electron doping) (Gao et al., 2011; Qi et al., 2012; Saha et al., 2012; Ying et al., 2012) and 38 K (for hole doping) (Rotter et al., 2008; Sasmal et al., 2008; Zhao et al., 2010). The superconducting phase in the RE-doped 122 (or A-doped 122 IBS) arises by the suppression of the SDW order via chemical pressure, electron (or hole) doping, or the combination of both (Saha et al., 2012). However, isovalent substitution of Ca^{2+} with Eu^{2+} neither adds any charge carriers

in the system nor suppresses the SDW order. As a result, no superconductivity has been observed in ECFA samples here. Nonetheless, ECFA provides a unique platform for studying magnetic orders arising from Eu^{2+} and Fe^{2+} sublattices. The doping dependence of T_{SDW} and T_N, as shown in Figure 3D, suggests that there exists a weak coupling between the SDW order of FeAs and Eu^{2+} localized moments. This result is consistent with NMR (Guguchia et al., 2011), neutron diffraction (Xiao et al., 2009), and ARPES (Zhou et al., 2010) studies on Eu122.

Summary

Magnetic properties of $Eu_xCa_{1-x}Fe_2As_2$ ($0 \leq x \leq 1$, ECFA) samples were presented. The resistivity data show clear anomalies due to the SDW and Eu^{2+} AFM transitions. The magnetic susceptibility (χ) of ECFA samples exhibits $1/T$ behavior, which can explained using the Curie-Weiss law. The χ (T) data provide evidence of the Eu^{2+} AFM order but do not indicate the SDW transition due to the Fe-moments. A weak transition near T_{SDW} appears only after the subtraction of the Curie-Weiss contribution of the Eu^{2+} moments. With increasing Eu doping, T_{SDW} initially increases rapidly up to $x \sim 0.4$, and it then gradually saturates to a value of 190 K at $x = 1$. The best-fits of the Curie-Weiss law parameters, the Curie constant (C), and the Weiss-temperature (θ), increase linearly with increasing Eu doping, while the effective magnetic moment, μ_{eff}, per Eu^2 + ion remains nearly constant. Our results provide detailed information about how the magnetic properties evolve in the Eu-doped Ca122 system, which will eventually help in understanding superconductivity in ECFA.

Data availability statement

The raw data supporting the conclusion of this article will be made available by the authors, without undue reservation.

Author contributions

BL synthesized high-quality samples of Eu-doped $CaFe_2As_2$. KS and LD carried out measurements. KS analyzed experimental data and wrote the manuscript. CC supervised the project.

Funding

The research at West Texas A&M University was supported by the Killgore Faculty Research program and the Welch Foundation (Grant No. AE-0025). The work done at the University of Houston was supported in part by U.S. Air Force Office of Scientific Research Grants FA9550-15-1-0236 and FA9550-20-1-0068, the T. L. L. Temple Foundation, the John J. and Rebecca Moores Endowment, and the State of Texas through the Texas Center for Superconductivity at the University of Houston. BL acknowledges financial support by U. S. Air Force Office of Scientific Research Grant FA9550-19-1-0037.

Conflict of interest

The authors declare that the research was conducted in the absence of any commercial or financial relationships that could be construed as a potential conflict of interest.

Publisher's note

References

Ashcroft and Mermin (1976). *Solid state physics*. New York: Holt Rinehart & Winston.

Chen, G. F., Li, Z., Wu, D., Li, G., Hu, W. Z., Dong, J., et al. (2008b). Superconductivity at 41 K and its competition with spin-density-wave instability in layered $CeO_{1-x}F_xFeAs$. *Phys. Rev. Lett.* 100, 247002. doi:10.1103/physrevlett.100.247002

Chen, X. H., Wu, T., Wu, G., Liu, R. H., Chen, H., and Fang, D. F. (2008a). Superconductivity at 43 K in $SmFeAsO_{1-x}F_x$. *Nature* 453, 761.

Deng, L., Bontke, T., Dahal, R., Xie, Y., Bin Gaoe, K. Y., Xue, Li, et al. (2021). Pressure-induced high-temperature superconductivity retained without pressure in FeSe single crystals. *Proc. Natl. Acad. Sci. U. S. A.* 118, e2108938118. doi:10.1073/pnas.2108938118

Deng, L. Z., Lv, B., Zhao, K., Wei, F. Y., Xue, Y. Y., Wu, Z., et al. (2016). Evidence for defect-induced superconductivity up to 49 K in $Ca_{1-x}R_xFe_2As_2$. *Phys. Rev. B* 93, 054513. doi:10.1103/physrevb.93.054513

Deng, L. Z., Lv, Z. W. B., Xue, Y. Y., Zhang, W. H., Li, F. S., Wang, L. L., et al. (2014). Meissner and mesoscopic superconducting states in 1–4 unit-cell FeSe films. *Phys. Rev. B* 90, 214513. doi:10.1103/physrevb.90.214513

Fernandes, R. M., Coldea, A. I., Ding, H., Fisher, I. R., Hirschfeld, P. J., and Kotliar, G. (2022). Iron pnictides and chalcogenides: A new paradigm for superconductivity. *Nature* 601, 35–44. doi:10.1038/s41586-021-04073-2

Gao, Z., Qi, Y., Wang, L., Wang, D., Zhang, X., Yao, C., et al. (2011). Synthesis and properties of La-doped $CaFe_2As_2$ single crystals with T_c = 42.7 K. *EPL* 95, 67002. doi:10.1209/0295-5075/95/67002

Guguchia, Z., Roos, J., Shengelaya, A., Katrych, S., Bukowski, Z., Weyeneth, S., et al. (2011). Strong coupling between Eu^{2+} spins and Fe_2As_2 layers in $EuFe_{1.9}Co_{0.1}As_2$ observed with NMR. *Phys. Rev. B* 83, 144516. doi:10.1103/physrevb.83.144516

Harnagea, L., Kumar, R., Singh, S., Wurmehl, S., Wolter, A. U. B., and Buchner, B. (2018). Evolution of the magnetic order of fe and eu sublattices in $Eu_{1-x}Ca_xFe_2As_2$

($0 \leq x \leq 1$) single crystals. *J. Phys. Condens. Matter* 30, 415601. doi:10.1088/1361-648x/aadea6

He, Y., Wu, T., Wu, G., Zheng, Q. J., Liu, Y. Z., Chen, H., et al. (2010). Evidence for competing magnetic and superconducting phases in superconducting $Eu_{1-x}Sr_xFe_{2-y}Co_yAs_2$ single crystals. *J. Phys. Condens. Matter* 22, 235701. doi:10.1088/0953-8984/22/23/235701

Herrero-Martín, J., Scagnoli, V., Mazzoli, C., Su, Y., Mittal, R., Xiao, Y., et al. (2009). Magnetic structure of $EuFe_2As_2$ as determined by resonant x-ray scattering. *Phys. Rev. B* 80, 134411. doi:10.1103/physrevb.80.134411

Hsu, F. C., Luo, J. Y., Yeh, K. W., Chen, T. K., Huang, T. W., Wu, P. M., et al. (2008). Superconductivity in the PbO-type structure alpha-FeSe. *Proc. Natl. Acad. Sci. U. S. A.* 105, 14262–14264. doi:10.1073/pnas.0807325105

Jeevan, H. S., Hossain, Z., Kasinathan, D., Rosner, H., Geibel, C., and Gegenwart, P. (2008). High-temperature superconductivity in $Eu_{0.5}K_{0.5}Fe_2As_2$. *Phys. Rev. B* 78, 092406. doi:10.1103/physrevb.78.092406

Jiang, S., Luo, Y., Ren, Z., Zhu, Z., Wang, C., Xu, X., et al. (2009). Metamagnetic transition in $EuFe_2As_2$ single crystals. *New J. Phys.* 11, 025007. doi:10.1088/1367-2630/11/2/025007

Kamihara, Y., Watanabe, T., Hirano, M., and Hosono, H. (2008). Iron-based layered superconductor $La[O_{1-x}F_x]Fe_2As_2$, x = 0.05 - 0.12 with T_c = 26 K. *J. Am. Chem. Soc.* 130, 3296.

Kittel, C. (2006). *Introduction to solid state physics*. Delhi: Pushp Print Service.

Komedera, K., Blachowski, A., Ruebenbauer, K., Zukrowski, J., Dubiel, S., Tran, L., et al. (2018). Mössbauer study of $Eu_{0.57}Ca_{0.43}Fe_2As_2$ and $Eu_{0.73}Ca_{0.27}(Fe_{0.87}Co_{0.13})_2$ As_2: A comparison to "122" iron-based superconductors parent compounds $EuFe_2As_2$ and $CaFe_2As_2$. *J. Magn. Magn. Mat.* 457, 1–7. doi:10.1016/j.jmmm.2018.02.079

Kurita, N., Kimata, M., Kodama, K., Harada, A., Tomita, M., Suzuki, H. S., et al. (2011). Phase diagram of pressure-induced superconductivity in $EuFe_2As_2$ probed by high-pressure resistivity up to 3.2 GPa. *Phys. Rev. B* 83, 214513. doi:10.1103/physrevb.83.214513

Lee, H., Park, E., Park, T., Sidorov, V. A., Ronning, F., Bauer, E. D., et al. (2009). Pressure-induced superconducting state of antiferromagnetic $CaFe_2As_2$. *Phys. Rev. B* 80, 024519. doi:10.1103/physrevb.80.024519

Lei, B., Cui, J. H., Xiang, Z. J., Shang, C., Wang, N. Z., Ye, G. J., et al. (2016). Evolution of high-temperature superconductivity from a low-T_c phase tuned by carrier concentration in FeSe thin flakes. *Phys. Rev. Lett.* 116, 077002. doi:10.1103/physrevlett.116.077002

Lv, B., Deng, L., Gooch, M., Wei, F., Sun, Y., Meen, J. K., et al. (2011). Unusual superconducting state at 49 K in electron-doped $CaFe_2As_2$ at ambient pressure. *Proc. Natl. Acad. Sci. U. S. A.* 108, 15705–15709. doi:10.1073/pnas.1112150108

Maiwald, J., and Gegenwart, P. (2017). Interplay of 4f and 3d moments in $EuFe_2As_2$ iron pnictides. *Phys. Status Solidi B* 254, 1600150. doi:10.1002/pssb.201600150

Park, T., Park, E., Lee, H., Klimczuk, T., Bauer, E. D., Ronning, F., et al. (2008). Pressure-induced superconductivity in $CaFe_2As_2$. *J. Phys. Condens. Matter* 20, 322204. doi:10.1088/0953-8984/20/32/322204

Qi, Y., Gao, Z., Wang, L., Wang, D., Zhang, X., and Ma, Y. (2008). Superconductivity at 34.7 K in the iron arsenide $Eu_{0.7}Na_{0.3}Fe_2As_2$. *New J. Phys.* 10, 123003. doi:10.1088/1367-2630/10/12/123003

Qi, Y., Gao, Z., Wang, L., Wang, D., Zhang, X., Yao, C., et al. (2012). Transport properties and anisotropy in rare-earth doped $CaFe_2As_2$ single crystals with T_c above 40 K. *Supercond. Sci. Technol.* 25, 045007. doi:10.1088/0953-2048/25/4/045007

Ren, Z., Zhu, Z., Jiang, S., Xu, X., Tao, Q., Wang, C., et al. (2008). Antiferromagnetic transition in $EuFe_2As_2$: A possible parent compound for superconductors. *Phys. Rev. B* 78, 052501. doi:10.1103/physrevb.78.052501

Rotter, M., Tegel, M., and Johrendt, D. (2008). Superconductivity at 38 K in the iron arsenide$(Ba_{1-x}K_x)Fe_2As_2$. *Phys. Rev. Lett.* 101, 107006. doi:10.1103/physrevlett.101.107006

Saha, S. R., Butch, N. P., Drye, T., Magill, J., Ziemak, S., Kirshenbaum, K., et al. (2012). Structural collapse and superconductivity in rare-earth-doped $CaFe_2As_2$. *Phys. Rev. B* 85, 024525. doi:10.1103/physrevb.85.024525

Sasmal, K., Lv, B., Lorenz, B., Guloy, A. M., Chen, F., Xue, Y.-Y., et al. (2008). Superconducting Fe-based compounds(A1−xSrx)Fe2As2withA=Kand Cs with transition temperatures up to 37 K. *Phys. Rev. Lett.* 101, 107007. doi:10.1103/physrevlett.101.107007

Shrestha, K., Deng, L. Z., Zhao, K., Jawdat, B. I., Lv, B., Lorenz, B., et al. (2020). Doping dependence and high-pressure studies on $Eu_xCa_{1-x}Fe_2As_2$ ($0 \leq x \leq 1$). *Supercond. Sci. Technol.* 33, 095010. doi:10.1088/1361-6668/ab9e7e

Takahashi, H., Igawa, K., Arii, K., Kamihara, Y., Hirano, M., and Hosono, H. (2008). Superconductivity at 43 K in an iron-based layered compound $Lao_{(1-x)}F_{(x)}$ FeAs. *Nature* 453, 376–378. doi:10.1038/nature06972

Terashima, T., Kimata, M., Satsukawa, H., Harada, A., Hazama, K., Uji, S., et al. (2009). $EuFe_2As_2$ under high pressure: An antiferromagnetic bulk superconductor. *J. Phys. Soc. Jpn.* 78, 083701. doi:10.1143/jpsj.78.083701

Torikachvili, M. S., Bud'ko, S. L., Ni, N., and Canfield, P. C. (2008). Pressure induced superconductivity in $CaFe_2As_2$. *Phys. Rev. Lett.* 101, 057006. doi:10.1103/physrevlett.101.057006

Tran, L. M., Babij, M., Korosec, L., Shang, T., Bukowski, Z., and Shiroka, T. (2018). Magnetic phase diagram of ca-substituted $EuFe_2As_2$. *Phys. Rev. B* 98, 104412. doi:10.1103/physrevb.98.104412

Wang, Q.-Y., Li, Z., Zhang, W.-H., Zhang, Z.-C., Zhang, J.-S., Li, W., et al. (2012). Interface-induced high-temperature superconductivity in single unit-cell FeSe films on $SrTiO_3$. *Chin. Phys. Lett.* 29, 037402. doi:10.1088/0256-307x/29/3/037402

Xiao, Y., Su, Y., Meven, M., Mittal, R., Kumar, C. M. N., Chatterji, T., et al. (2009). Magnetic structure of $EuFe_2As_2$ determined by single-crystal neutron diffraction. *Phys. Rev. B* 80, 174424. doi:10.1103/physrevb.80.174424

Xiao, Y., Su, Y., Schmidt, W., Schmalzl, K., Kumar, C. M. N., Price, S., et al. (2010). Field-induced spin reorientation and giant spin-lattice coupling in $EuFe_2As_2$. *Phys. Rev. B* 81, 220406. doi:10.1103/physrevb.81.220406

Ying, J. J., Liang, J. C., Luo, X. G., Wang, X. F., Yan, Y. J., Zhang, M., et al. (2012). Transport and magnetic properties of La-doped $CaFe_2As_2$. *Phys. Rev. B* 85, 144514. doi:10.1103/physrevb.85.144514

Ying, J. J., Wu, T., Zheng, Q. J., He, Y., Wu, G., Li, Q. J., et al. (2010). Electron spin resonance in $EuFe_{2-x}Co_xAs_2$ single crystals. *Phys. Rev. B* 81, 052503. doi:10.1103/physrevb.81.052503

Yu, W., Aczel, A. A., Williams, T. J., Bud'ko, S. L., Ni, N., Canfield, P. C., et al. (2009). Absence of superconductivity in single-phase $CaFe_2As_2$ under hydrostatic pressure. *Phys. Rev. B* 79, 020511. doi:10.1103/physrevb.79.020511

Zhang, M., Ying, J. J., Yan, Y. J., Wang, A. F., Wang, X. F., Xiang, Z. J., et al. (2012). Phase diagram as a function of doping level and pressure in the $Eu_{1-x}La_xFe_2As_2$ system. *Phys. Rev. B* 85, 092503. doi:10.1103/physrevb.85.092503

Zhao, K., Liu, Q. Q., Wang, X. C., Deng, Z., Lv, Y. X., Zhu, J. L., et al. (2010). Superconductivity above 33 k in $(Ca_{1-x}Na_x)Fe_2As_2$. *J. Phys. Condens. Matter* 22, 222203. doi:10.1088/0953-8984/22/22/222203

Zhao, K., Lv, B., Deng, L., Huyan, S.-Y., Xue, Y.-Y., and Chu, C.-W. (2016). Interface-induced superconductivity at 25 K at ambient pressure in undoped $CaFe_2As_2$ single crystals. *Proc. Natl. Acad. Sci. U. S. A.* 113, 12968–12973. doi:10.1073/pnas.1616264113

Zhou, B., Zhang, Y., Yang, L.-X., Xu, M., He, C., Chen, F., et al. (2010). High-resolution angle-resolved photoemission spectroscopy study of the electronic structure of $EuFe_2As_2$. *Phys. Rev. B* 81, 155124. doi:10.1103/physrevb.81.155124